

# Effect of remelting power and remelting time on the morphological characteristics and mechanical properties of Fe-based clad layer

Wenchao Xi <sup>a,b</sup>, Boxue Song <sup>c</sup>, Zhengyu Sun <sup>a</sup>, Zhelun Ma <sup>a</sup>, Tianbiao Yu <sup>a,\*</sup>, Jun Wang <sup>a</sup>

<sup>a</sup> School of Mechanical Engineering and Automation, Northeastern University, PR China

<sup>b</sup> School of Mechanical and Aerospace Engineering, Nanyang Technological University, Singapore

<sup>c</sup> School of Mechanical Engineering, Shenyang University of Technology, PR China

## ARTICLE INFO

### Keywords:

Laser remelting  
Remelting power  
Remelting time  
Morphological characteristics  
Wear mechanisms

## ABSTRACT

Laser remelting is a processing technique to improve the quality of forming. The remelting power and the remelting time are the key factors affecting its processing quality. Laser remelting tests were conducted on Fe-based clad layers with different remelting power and remelting time, and the morphological characteristics of each clad layer was investigated by laser microscopy. The microhardness, wear resistance and wear mechanism of each clad layer were investigated by Vickers microhardness tester and reciprocating friction and wear tester, respectively. The results show that an increase in remelting power or remelting time leads to a decrease in clad height and an increase in melting pool depth, clad width and dilution rate. When the remelting time is 1 and the remelting power is 650 W, the clad height is higher than that of YCF102 clad layer, although the melting pool depth, clad width and dilution rate of the clad layer are greater than that of YCF102 clad layer. In addition, an increase in remelting power or remelting times leads to a decrease in the microhardness of the clad layer and a deterioration in the wear resistance, which leads to an increase in the wear rate, but does not change the trend of microhardness, wear resistance and wear rate. Neither the increase in remelting power nor the remelting time leads to a change in the wear form, but causes the wear between the clad layer and the grinding ball to become more intense. The clad layer with 1 remelting time and 650 W remelting power has higher average microhardness and more outstanding wear resistance than the YCF102 clad layer.

## 1. Introduction

Laser remelting is a process in which the surface of the clad layer is rapidly melted and solidified by the radiation of a laser beam without the addition of any metallic elements [1,2]. This processing method has the advantages of a small heat-affected zone, ease of operation, and controllability of processing quality [3,4]. When laser cladding is implemented, defects such as sticky powder located on the surface of the clad layer and pores or cracks located inside the clad layer often occur [5,6]. Although methods such as milling, grinding, polishing and optimization of the laser cladding process parameters are potential options to solve these problems, the hindrances such as the limited location to be machined and the irregularity of the machined area led to the inability to guarantee the quality of the process [7,8]. Given the ability of laser remelting to refresh the solidification process of the clad layer, it gives the potential ability to change the surface quality and properties of the cladding layer.

There is a close relationship between laser remelting and the surface quality and corrosion resistance of the coating. Richter et al. [9] de-

veloped a model of laser remelting, and confirmed that laser remelting resulted in a more uniform distribution of elements and compounds, which led to a flatter surface topography. Gok et al. [10] proposed that suitable remelting parameters can refine the coating organization and reduce the surface roughness. Qunshuang et al. [11] demonstrated that remelting not only resulted in a more uniform distribution of carbides in the coating, but also changed the shape of carbides from irregular to polygonal. Matějčíček and Holub [12] confirmed that spot diameter and scan speed had a significant effect on the surface quality. Das et al. [13] pointed out that remelting can eliminate the number of holes and reduce porosity. Gao et al. [14] demonstrated that remelting can significantly improve the coating finish and reduce the cost of post-processing. Amaya-Vazquez et al. [15] proposed that remelting led to not only changes in microstructure, but also changes in corrosion resistance. Wang et al. [16] demonstrated that remelting can enhance the positive corrosion sites and reduce the corrosion current density of Ni-Cr-Mo coatings, thus improving the corrosion resistance of the coatings. Wang et al. [17] showed that although remelting leads to the reduction of amorphous content in the coating and the reduction of defects such as cracks and pores on the surface of the coating to improve the corrosion resistance of the coating, it also leads to trans granular cracks in the coating. Tian et al. [18] showed that although defects such as cracks and

\* Corresponding author.

E-mail address: [neutianbiaoyu2018@gmail.com](mailto:neutianbiaoyu2018@gmail.com) (T. Yu).

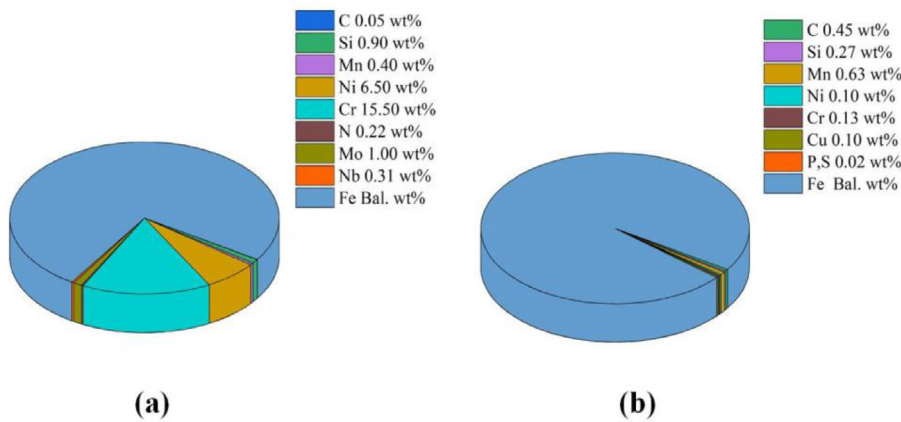


**Fig. 1.** Chemical composition of (a) YCF102 alloy powder and (b) AISI1045 steel (wt%) (Provided by manufacturer).

porosity still existed in the remelted coatings, remelting still improved the surface properties of the coatings.

In addition, remelting has an effect not only on the surface quality and corrosion resistance of the coating, but also on the mechanical properties of the coating significantly [19]. Iwaszko [20] showed that remelting significantly reduced the porosity of coatings and improved the mechanical properties of coatings. Cai et al. [21] suggested that remelting significantly reduced the wear quality loss and improved the wear resistance of coatings made of high-entropy alloys (Ni-Cr-Co-Ti-V). Habib et al. [22] proposed that remelting also significantly reduces the accumulated wear of coatings under lubricated conditions. Cai et al. [23] demonstrated that remelting significantly improved the spheroidization rate, size uniformity, and particle distribution of ceramic particles in the coating, which reduced the surface stress of the coating and thus improved the wear resistance of the coating. Mukherjee et al. [24] investigated the relationship between remelting power and wear resistance of coatings and showed that appropriate remelting power significantly reduced the wear depth of coatings and improved the wear resistance of coatings. Gao et al. [25] suggested that remelting improves the mechanical properties of coatings because of the denser columnar crystal zone in remelted coatings. Ciubotariu et al. [26] showed that remelting not only refines the coating microstructure but also improves the cavitation resistance of the coating.

In summary, the current research on laser remelting is mainly focused on the effects of remelting on the surface quality of the coating, the effects of remelting on the properties of the coating, and the relationship among the remelting power, the surface quality and properties of the coating, while the research on the effect of remelting power and remelting time on the morphological characteristics and mechanical properties of coating is still limited. In this study, single-factor remelting tests were conducted on YCF102 clad layers using different remelting power and remelting times, and the forming characteristics of each clad layer were investigated by measuring the clad width, clad height, melting pool depth and dilution rate of each layer. The mechanical properties and wear mechanism of the remelted clad layers were investigated by observing and calculating the microhardness, real-time friction coefficient curve, wear profile and wear rate under different remelting time and remelting power conditions. Finally, the clad layer with good morphology and mechanical properties were obtained.

## 2. Research methodology

A diode-pumped near-infrared fiber continuous-wave laser generator (YLR-1000 W) with a spot diameter of 1.1 mm and a laser wavelength range of 1070 nm to 1080 nm was used for the test. The alloy powder is injected into the laser beam in a coaxial feeding pattern and is coated on the substrate surface. In this case, the powder is injected at an angle of 31.41° and the powder carrier gas is argon with 99.99% pu-

rity. Also, argon was used as a barrier gas to stop the oxidation reaction during the laser cladding process. The flow rate of the barrier gas was 12 L/min and the distance between the laser nozzle and the substrate was 16 mm. The laser head is mounted on a vertical machining center (VMC1100P). A water-cooling system is installed in the laser cladding system in order to ensure that the laser cladding system is in the right operating temperature range under all operating conditions.

AISI1045 steel was selected as the base material. The surface of the substrate is milled by a milling machine and the surface is ground by metallographic sandpaper to achieve a flat substrate surface. In order to remove the dirt and oil residues on the substrate surface during processing, acetone and alcohol solvents were successively used to clean the substrate surface. The test used YCF102 iron-based alloy powder, which has the advantages of low cost and good mechanical properties. The composition of the substrate material and YCF102 alloy powder is shown in Fig. 1.

In a previous study by the authors [27], when the laser power was 750 W, the powder feeding rate was 7 g/min, the laser scanning speed was 4 mm/s, and the remelting laser power was 650 to 850 W, the clad layer had a good surface morphology. Therefore, the process parameters used in this paper are shown in Table 1. In order to analyze and study the cross sections of the samples, each sample was first wire cut by wire EDM (WEDM), and then each sample was etched by aqua regia. Finally, the cross-sectional parameters and cross-sectional microstructure of each sample were obtained by Olympus three-dimensional measurement laser microscope (OLS4100), and the microhardness of each sample was measured by Vickers microhardness tester (MH-500). The loading force was 10 N and the loading time was 15 s. The top layer of each sample was removed by grinding machine, and the top surface of each sample was sanded and polished by metallographic sandpaper and polishing machine successively. Reciprocating friction and wear tests were performed on each sample by a multifunctional material surface property tester (MFT-4000), and the parameters of the reciprocating friction and wear tests are shown in Table 2. The wear volume and wear morphology of each sample were obtained by Olympus three-dimensional measurement laser microscope (OLS4100).

## 3. Results and discussion

### 3.1. Morphological characteristics parameters and dilution rate of the clad layer

Figs. 2 and 3 show the morphological characteristics parameters and dilution rates of the  $L_0^0$  clad layer and clad layer after remelting with different remelting power and remelting times, respectively. From Fig. 2(a), it can be seen that when the remelting time is 1 s, the clad width and melting pool depth show a monotonic increasing trend with the increase of remelting power, but the clad height shows a decreasing

**Table 1**  
The process parameters of laser cladding and remelting.

| No. | Laser power (W) | Powder feeding rate (g/min) | Laser scanning velocity(mm/s) | Re-melting laser power (W) | Re-melting laser scanning velocity (mm/s) | Number of re-melting | Work condition of tag |
|-----|-----------------|-----------------------------|-------------------------------|----------------------------|---|----------------------|-----------------------|
| 1   | 750             | 7                           | 4                             | -                          | -   | -                    | $L_0^0$               |
| 2   | 750             | 7                           | 4                             | 650                        | 4   | 1                    | $L_{650}^1$           |
| 3   | 750             | 7                           | 4                             | 650                        | 4   | 2                    | $L_{650}^2$           |
| 4   | 750             | 7                           | 4                             | 650                        | 4   | 3                    | $L_{650}^3$           |
| 5   | 750             | 7                           | 4                             | 750                        | 4   | 1                    | $L_{750}^1$           |
| 6   | 750             | 7                           | 4                             | 750                        | 4   | 2                    | $L_{750}^2$           |
| 7   | 750             | 7                           | 4                             | 750                        | 4   | 3                    | $L_{750}^3$           |
| 8   | 750             | 7                           | 4                             | 850                        | 4   | 1                    | $L_{850}^1$           |
| 9   | 750             | 7                           | 4                             | 850                        | 4   | 2                    | $L_{850}^2$           |
| 10  | 750             | 7                           | 4                             | 850                        | 4   | 3                    | $L_{850}^3$           |

Note: The working condition mark L in Table 1 represents the number of times without remelting and different remelting power and remelting times. The superscript of L is the remelting time and the subscript is the remelting power.  $L_0^0$  indicates no remelting. When changing the remelting time and remelting power, the powder feeding rate is 0 g/min and the laser scanning speed is kept constant.

**Table 2**  
Wear parameters of the YCF102 clad layer with different remelting power and remelting times.

| Wear parameters | Load | Wear time | Wear distance | Wear velocity | Diameter of the grinding ball | Material of grinding ball |
|-----------------|------|-----------|---------------|---------------|-------------------------------|---------------------------|
| Value           | 10 N | 40 min    | 5 mm          | 240 mm/s      | 4 mm                          | GCr15                     |

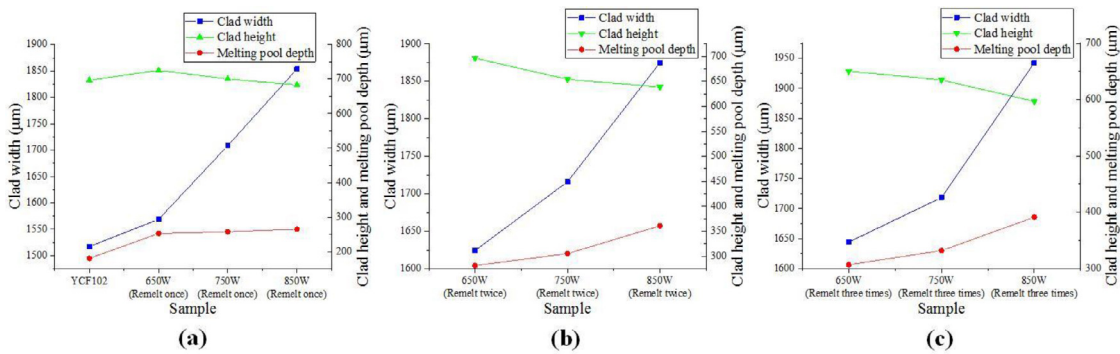


**Fig. 2.** Characteristic parameters of the clad layer morphology (a) No remelting and remelting once with different remelting power (b) Remelting twice with different remelting power (c) Remelting three times with different remelting power.

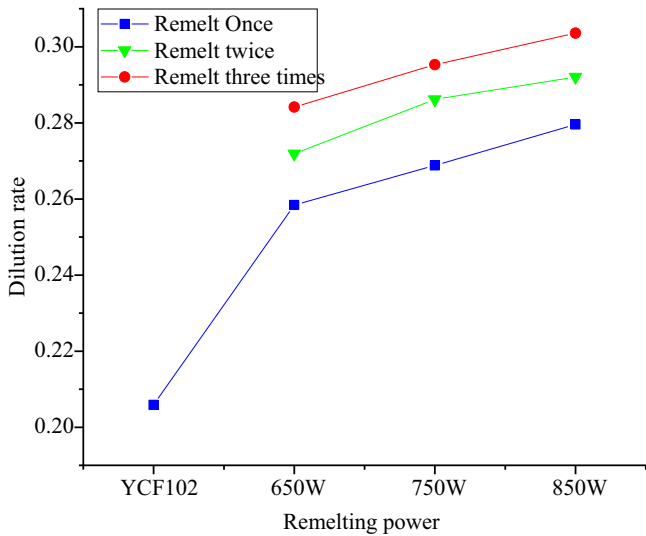


**Fig. 3.** Dilution rate of YCF102 clad layer without remelting and after remelting under different remelting power and remelting time conditions.

trend. The clad height of the  $L_{650}^1$  clad layer is higher than that of the  $L_0^0$  clad layer. However, the clad heights of the  $L_{750}^1$  and  $L_{850}^1$  clad layers are lower than that of the  $L_0^0$  clad layer. This phenomenon may be attributed

to the fact that when the surface of the YCF102 clad layer is again radiated by the laser beam, the incompletely melted powder on the surface is melted and a clad layer is formed, resulting in a higher clad height of the  $L_{650}^1$  clad layer than that of the  $L_0^0$  clad layer. When the remelting power is further increased, more of the substrate is melted, resulting in more YCF102 clad layer fused into the substrate. When the mass of YCF102 clad layer fused to the substrate due to remelting exceeds the mass of the incompletely melted powder forming the clad layer, the clad height shows a decreasing trend. Therefore, the clad heights of the  $L_{750}^1$  and  $L_{850}^1$  clad layers are lower than that of the  $L_0^0$  clad layer. At the same time, the increase in remelting power leads to the melting of the YCF102 clad layer as well as more of the substrate, resulting in the same trend of increasing clad width and melting pool depth.

As can be seen from Fig. 2, when the remelting time is 1, 2 and 3, respectively, the clad height shows a decreasing trend with the increase of remelting power, while the clad width and melting pool depth both show an increasing trend. The results show that the increase of remelting time does not change the trend of the morphological parameters of the clad layer with the remelting power. Meanwhile, when the remelting power is 650 W, 750 W and 850 W, respectively, the clad height shows a decreasing trend with the increase of remelting time, while the clad width and melting pool depth both show an increasing trend. The results showed that the change of remelting power also does not change the trend of the morphological parameters of the clad layer with the remelting time. Therefore, although the increase of both remelting power and remelting time leads to the change of the morphological pa-

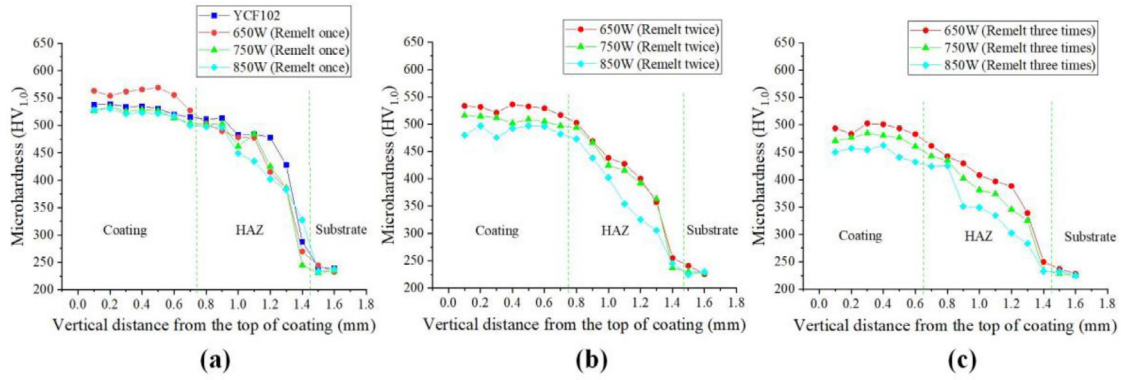


Fig. 4. Microhardness of the clad layer at different depths (a) No remelting and remelting once with different remelting power (b) Remelting twice with different remelting power (c) Remelting three times with different remelting power.

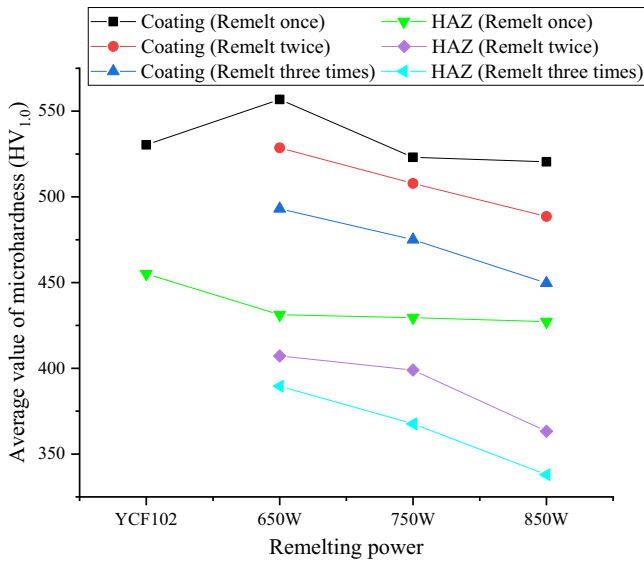


Fig. 5. Average microhardness of the clad layer without remelting and after remelting with different remelting power and remelting times.

rameters of the clad layer, it does not affect the change the trend of the morphological parameters of the clad layer.

As can be seen from Fig. 3, when the remelting time is kept constant, the dilution rate shows an increasing trend with the increase of remelting power. When the remelting power is kept constant, the dilution rate also shows an increasing trend with the increase of remelting time. This phenomenon is due to the fact that the increase in remelting power and remelting time both result in more YCF102 clad layer incorporated into the substrate, which leads to an increase in dilution rate. In addition, the dilution rate of the  $L_{650}^1$  clad layer is higher than that of the  $L_0^0$  clad layer. This phenomenon is due to the fact that under  $L_{650}^1$  condition, the increase in clad height due to remelting is smaller than the increase in melting pool depth, which leads to an increase in dilution rate.

### 3.2. Microhardness of the clad layer

Figs. 4 and 5 show the microhardness and average microhardness of the clad layer at different depths of  $L_0^0$  clad layer and clad layers after remelting with different remelting power and remelting times, respectively. From Figs. 4(a) and 5, it can be seen that the average microhardness of the  $L_{650}^1$  clad layer is higher than the average microhardness of the  $L_0^0$  clad layer, while the average microhardness of both the  $L_{750}^1$  and  $L_{850}^1$  clad layers is lower than the average microhardness of the  $L_0^0$

clad layer. Meanwhile, it can be seen from Figs. 4 and 5 that the average microhardness all showed a decreasing trend with the increase of remelting power when the remelting time is 1, 2 and 3, respectively. This phenomenon may be explained by the fact that when the laser beam with a remelting power of 650 W passes over the surface of the YCF102 clad layer, the powder adhering to the surface is melted and a clad layer is formed, resulting in the disappearance of defects and the expulsion of gasses that have not been completely expelled from the clad layer. At the same time, the remelting acts as a fine grain reinforcement, which leads to an increase in the average microhardness. However, with further increase in remelting power, the effect of heat accumulation due to remelting and thus the grain size in the clad layer becomes larger. As a result, the average microhardness shows a decreasing trend with increasing remelting power. From Figs. 4 and 5, it can be seen that when the remelting power is 650 W, 750 W and 850 W, respectively, the average microhardness shows a decreasing trend with the increase of remelting time. This phenomenon is due to the increase in the remelting time, which leads to the increase in the heat accumulated in the clad layer, resulting in a smaller temperature difference and lower cooling rate. As a result, it leads to larger grains and a decrease in the average microhardness.

In addition, it can be seen from Fig. 4 that the microhardness curves of both the  $L_0^0$  clad layer and the clad layer after remelting with different remelting time and remelting power conditions show a continuous variation. The results show that each clad layer forms a good metallurgical bond with the substrate. At the same time, the average microhardness of the heat affected zone (HAZ) of each sample is higher than the average microhardness of the substrate due to fine grain strengthening and solid solution strengthening.

### 3.3. Tribological properties of the clad layer

Figs. 6(b), 7(b) and 8(b) show the real-time friction coefficients of  $L_0^0$  clad layer and clad layers after remelting with different remelting power and remelting times, where the real-time friction coefficients for wear times from 0 to 1 min are shown in Figs. 6(a), 7(a) and 8(a). The results show that the friction coefficient of  $L_0^0$  clad layer and clad layers after remelting with different remelting power and remelting times showed a short "plateau" period with small fluctuations at the beginning of wear. This phenomenon is caused by the fact that the surface of each clad layer is processed by wire cutting, grinding and polishing in order to ensure the surface flatness of each sample before the friction wear test. During the process, a hard processing layer is created on the surface of each sample. As a result, a short "plateau" period was observed in the real-time friction coefficient curves of each sample at the beginning of the wear phase. At the same time, the length of the "plateau" period varied from sample to sample due to the different thickness of the hard processing layer. When the hard processing layer of each sample is worn

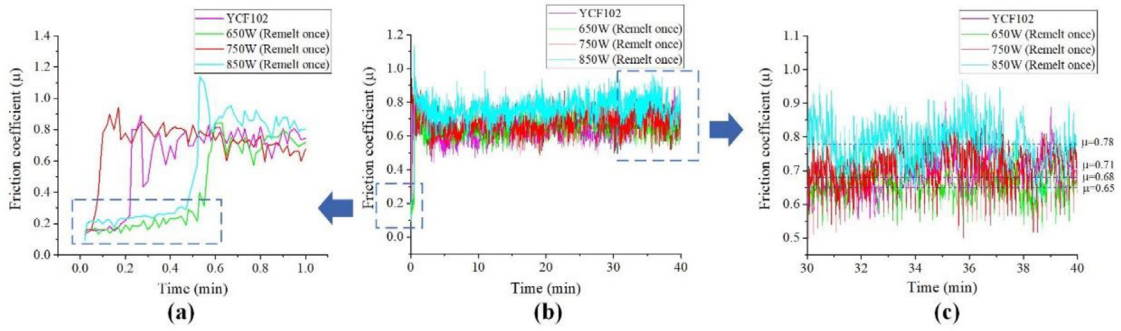


Fig. 6. Friction coefficient of the clad layer without remelting and after remelting once with different power (a) Wear time of 0–1 min (b) Wear time of 0–40 min (c) Wear time of 30–40 min.

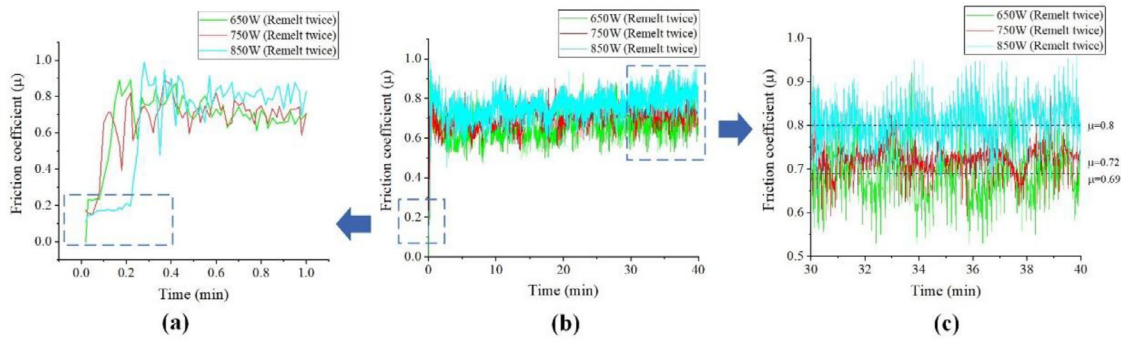


Fig. 7. Friction coefficient of the clad layer after remelting twice with different power (a) Wear time of 0–1 min (b) Wear time of 0–40 min (c) Wear time of 30–40 min.

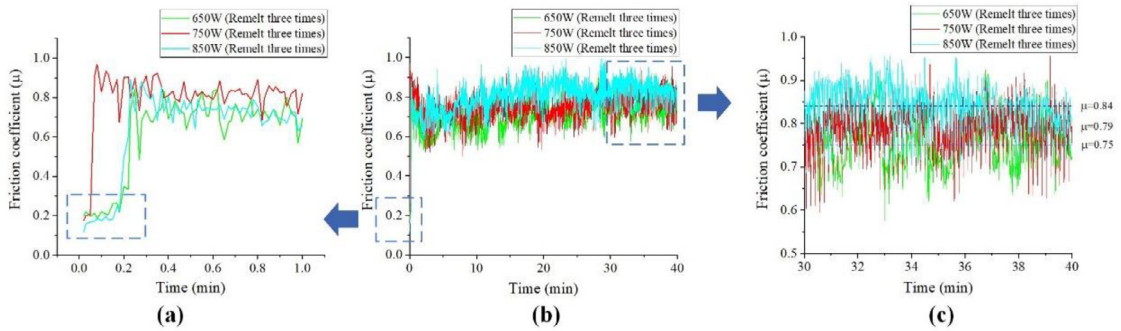


Fig. 8. Friction coefficient of the clad layer after remelting three times with different power (a) Wear time of 0–1 min (b) Wear time of 0–40 min (c) Wear time of 30–40 min.

away, the friction coefficient increases significantly and undergoes large fluctuations. At this time, each sample is in the stage of intense friction. With the increase of the wear time, the fluctuation of the real-time friction coefficient gradually tends to be smooth. At this point, each sample is in the stable friction stage. The real-time friction coefficient as well as the average friction coefficient of each sample in the wear time interval of 30 to 40 min were selected to study the wear resistance of each sample.

As shown in Fig. 6(c), the average friction coefficients of the  $L_0^0$  clad layer and clad layers after remelting once with different remelting power conditions are in the following order:  $L_{650}^1 < L_0^0 < L_{750}^1 < L_{850}^1$ . The average friction coefficient of the  $L_{650}^1$  clad layer is lower than the average friction coefficient of the  $L_0^0$  clad layer. Also, the average friction coefficient of this clad layer is the minimum value of the average friction coefficient of all samples. However, the average friction coefficients of the  $L_{750}^1$  and  $L_{850}^1$  clad layers are higher than the average friction coefficients of the  $L_0^0$  clad layer. Moreover, as shown in Figs. 6(c), 7(c) and 8(c), the average friction coefficient shows an increasing trend with the increase

of remelting power when the remelting time is kept constant. This phenomenon is due to the fact that the average microhardness of the  $L_{650}^1$  clad layer is higher than the average microhardness of the  $L_0^0$  clad layer, so the average friction coefficient is lower than the average friction coefficient of the  $L_0^0$  clad layer, and has better wear resistance. And with the increase of remelting power, the average microhardness shows a decreasing trend. As a result, the average friction coefficient tends to increase and leads to the deterioration of wear resistance. As shown in Figs. 6(c), 7(c) and 8(c), when the remelting power is kept constant, the average friction coefficient shows an increasing trend with the increase of remelting time. This phenomenon is attributed to the decrease of the average microhardness with the increase of the remelting time when the remelting power is kept constant. Therefore, the wear resistance becomes worse with the increase of remelting time. In addition, as can be seen from Figs. 6–8, an increase in the remelting time or remelting power leads to an increase in the average friction coefficient and a deterioration in wear resistance. However, changing the remelting time does not have a significant effect on the variation pattern of the average fric-

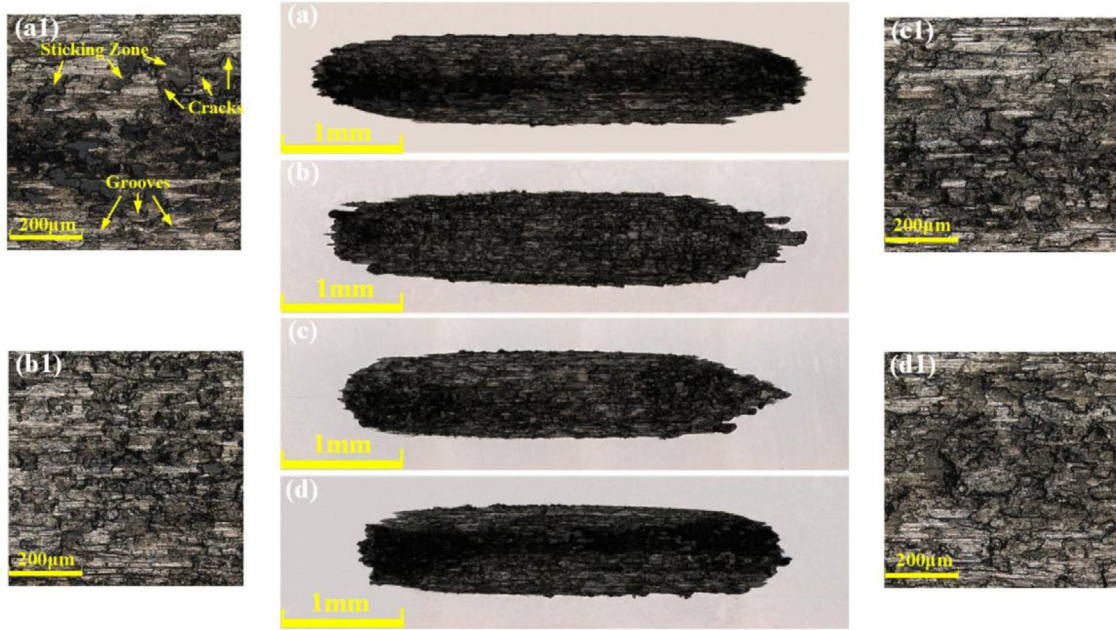


Fig. 9. Wear morphology of the clad layer without remelting and after remelting once with different power (a) No remelting (b) Remelting power is 650 W (c) Remelting power is 750 W (d) Remelting power is 850 W.

tion coefficient with remelting power. Similarly, changing the remelting power does not significantly affect the variation pattern of the average friction coefficient with the remelting time.

Fig. 9 shows the wear morphology of the  $L_0^0$  clad layer and the clad layer after remelting once with different remelting power. As shown in Figs. 9(a1)–(d1) and 12, more cracks are found in each wear morphology. The occurrence of friction between grinding ball and surface asperities causes the surface of sample to be in alternative compressive-tensile stress state, which leads to the development of cracks. Therefore, surface fatigue wear occurs on the clad layers. Also, more abrasive chips and grooves are found in each wear morphology. This phenomenon may be caused by the formation of abrasive chips between the grinding ball and the clad layer when wear occurs. These chips roll and slide reciprocally on the surface of the clad layer, resulting in the occurrence of plastic deformation and the formation of grooves on the wear surface. A part of chips is embedded in the wear surface under the action of load and friction force. It shows that abrasive wear is also occurring during the wear process. In addition, sticking zones are found in the wear morphology. This indicates that a portion of the clad layer adheres to the grinding ball when wear occurs. As the wear progressed, the shearing phenomenon occurs due to the relative sliding of the adhered parts. As a result, adhesive wear occurs between the grinding ball and the clad layer.

Figs. 10–12 show the wear morphology after two and three remelts for different remelting power conditions, respectively. There are a large number of sticking zones, cracks, grooves and abrasive chips on the wear surface. The results show that the increase in remelting time does not lead to a change in the wear forms of the clad layers. However, as shown in Figs. 10(c1) and 11(c1), deeper grooves and more sticking zones were found in the central region of the wear morphology of the  $L_{850}^2$  and  $L_{850}^3$  clad layers. This phenomenon is due to the tendency of the average microhardness to decrease with the increase of remelting power or remelting times. When the wear parameters are kept constant, the volume of the grinding ball embedded in the clad layer increases with the decrease of the average microhardness, leading to the above phenomenon. Furthermore, as shown in Figs. 9(d1), 10(c1) and 11(c1), when the remelting power is kept constant, the grooves at the central region of the wear morphology become wider and deeper with the increase of the remelt-

Table 3

EDS analysis results of clad layer after wear with different remelting power and remelting times.

| Sample      | Point | Fe    | Cr    | Ni   | Si   | O     |
|-------------|-------|-------|-------|------|------|-------|
| $L_0^0$     | A     | 65.49 | 13.13 | 6.02 | 0.88 | 14.48 |
|             | B     | 75.37 | 16.49 | 6.70 | 0.93 | 0.51  |
|             | C     | 67.01 | 14.83 | 6.24 | 1.01 | 10.91 |
| $L_{650}^1$ | A     | 64.82 | 12.84 | 5.55 | 0.66 | 16.13 |
|             | B     | 77.73 | 13.30 | 6.88 | 0.79 | 1.30  |
|             | C     | 71.99 | 11.75 | 5.04 | 0.33 | 10.89 |
| $L_{650}^2$ | A     | 70.39 | 11.49 | 5.40 | 0.72 | 12.00 |
|             | B     | 79.83 | 12.81 | 6.22 | 0.70 | 0.44  |
|             | C     | 72.75 | 12.21 | 5.35 | 0.58 | 9.11  |
| $L_{650}^3$ | A     | 69.05 | 12.23 | 5.60 | 0.76 | 12.36 |
|             | B     | 77.18 | 14.29 | 7.04 | 0.88 | 0.61  |
|             | C     | 71.57 | 11.92 | 5.57 | 0.77 | 10.17 |
| $L_{750}^1$ | A     | 70.76 | 13.02 | 6.35 | 0.73 | 9.14  |
|             | B     | 77.09 | 14.17 | 7.07 | 0.80 | 0.87  |
|             | C     | 72.77 | 14.45 | 5.55 | 0.47 | 6.76  |
| $L_{750}^2$ | A     | 66.86 | 12.21 | 5.98 | 0.72 | 14.23 |
|             | B     | 77.19 | 14.24 | 6.97 | 0.76 | 0.84  |
|             | C     | 69.51 | 13.11 | 5.67 | 0.50 | 11.21 |
| $L_{750}^3$ | A     | 68.61 | 12.22 | 5.96 | 0.78 | 12.43 |
|             | B     | 78.61 | 13.53 | 6.59 | 0.85 | 0.42  |
|             | C     | 69.70 | 14.15 | 5.47 | 0.26 | 10.42 |
| $L_{850}^1$ | A     | 69.40 | 12.67 | 6.02 | 0.77 | 11.14 |
|             | B     | 77.91 | 13.68 | 6.54 | 0.85 | 1.02  |
|             | C     | 71.88 | 13.60 | 6.23 | 0.65 | 7.64  |
| $L_{850}^2$ | A     | 66.20 | 13.02 | 5.99 | 0.72 | 14.07 |
|             | B     | 78.27 | 13.55 | 6.85 | 0.74 | 0.59  |
|             | C     | 70.18 | 13.38 | 5.87 | 0.62 | 9.95  |
| $L_{850}^3$ | A     | 67.43 | 11.36 | 5.73 | 0.68 | 14.80 |
|             | B     | 78.52 | 13.20 | 6.66 | 0.80 | 0.82  |
|             | C     | 70.15 | 11.94 | 5.57 | 0.69 | 11.65 |

ing times. This result indicates that when the remelting power is kept constant, the increase in the remelting times leads to more intense wear between the clad layer and the grinding ball.

Fig. 12 and Table 3 show the results of EDS analysis of wear morphology of  $L_0^0$  clad layer and the clad layer after remelting with different remelting power and remelting times, respectively. The results show that wear surface undergo oxidation reactions and form oxide films dur-

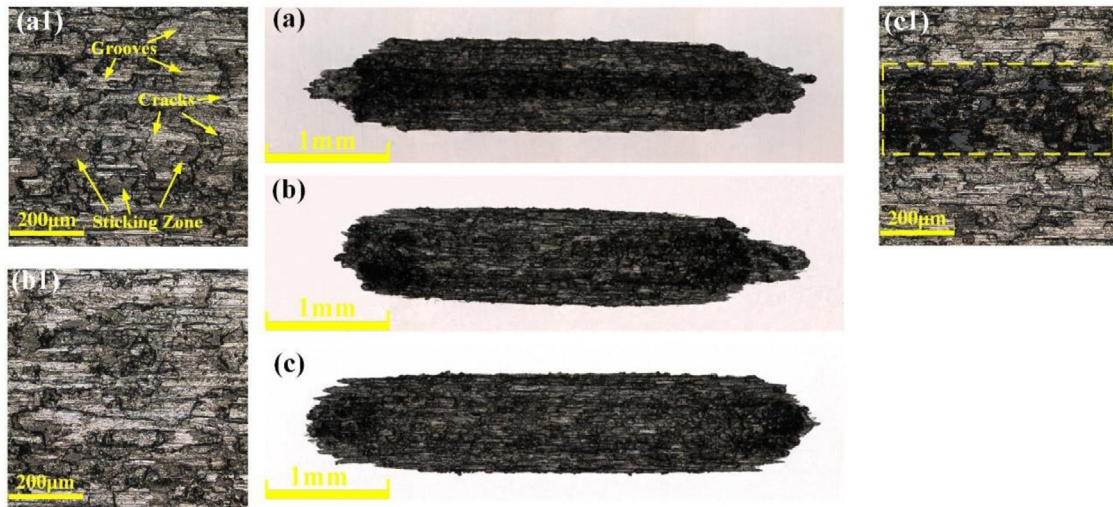


Fig. 10. Wear morphology of the clad layer after remelting twice with different power (a) No remelting (b) Remelting power is 650 W (c) Remelting power is 750 W (d) Remelting power is 850 W.

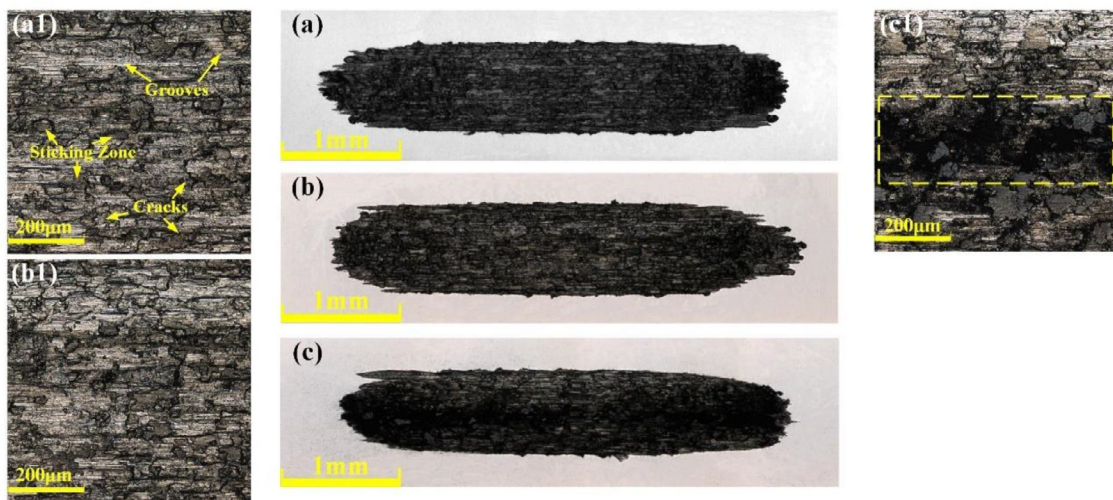


Fig. 11. Wear morphology of the clad layer after remelting three times with different power (a) No remelting (b) Remelting power is 650 W (c) Remelting power is 750 W (d) Remelting power is 850 W.

ing the wear process, but the oxide films are not continuous. It can be seen from Fig. 12 and Table 3 that the sticking zone (A) has a higher oxygen content. The results show that continuous oxide films are formed on the sticking zone of each sample. The reason for this phenomenon is that when the frictions occur between the surface of clad layer and grinding ball, a portion of clad layer adheres to grinding ball and then is sheared away with the reciprocating motion. The sheared surface undergoes oxidation reaction and forms oxide films under the promotion of friction heat. In addition, it can be seen from Fig. 12 and Table 3 that the oxygen content in sticking zone (A) and abrasive chips (C) is higher than that of groove zone (B). The results show that oxide films are formed on the wear surface, but the rate of formation is lower than that of removal. When the critical thickness is reached, the oxide film fractures and abrasive chips are formed. As a result, the oxygen content in groove zones is lower and the oxide film of wear surface is not continuous. The alternation between formation and fracture of oxide films is one of the factors leading to the fluctuation of friction coefficient. According to the previous literature, the composition of oxide film is  $\text{Fe}_3\text{O}_4$  and  $\text{Fe}_2\text{O}_3$  [28]. In addition, it can be seen from Figs. 9–12 that despite the changes of remelting power and remelting time, a large number of sticking zones, cracks, grooves and abrasive chips are found on wear morphology of

each sample. The results show that surface fatigue wear, abrasive wear, adhesive wear and oxidative wear occur during the wear process. Changing the remelting power or remelting time does not change the wear form.

Based on the wear morphology and the results of EDS analysis, the wear mechanism of each sample is shown in Fig. 13. The wear surface undergoes plastic deformation during the wear process, and the local bulge occurs near two end points of wear track. The friction between grinding ball and surface asperities causes the wear surface to be in an alternating state of compressive stress and tensile stress, which leads to the formation of cracks. During the wear process, oxide films are formed on the wear surface. Meanwhile, the generation of friction heat leads to an increase in the formation rate of oxide films. However, the formation rate of oxide films is lower than the removal rate, so a portion of clad layer is spalled off and abrasive chips are formed. Among them, part of chips accumulate near two end points of wear track. part of chips roll and slide between grinding ball and clad layer, which leads to the fracture of oxide films and the formation of grooves. When the chips roll and slide between grinding ball and clad layer, a portion of chips collapses and forms smaller chips under the action of friction force and load. At the same time, some of chips are embedded in the wear

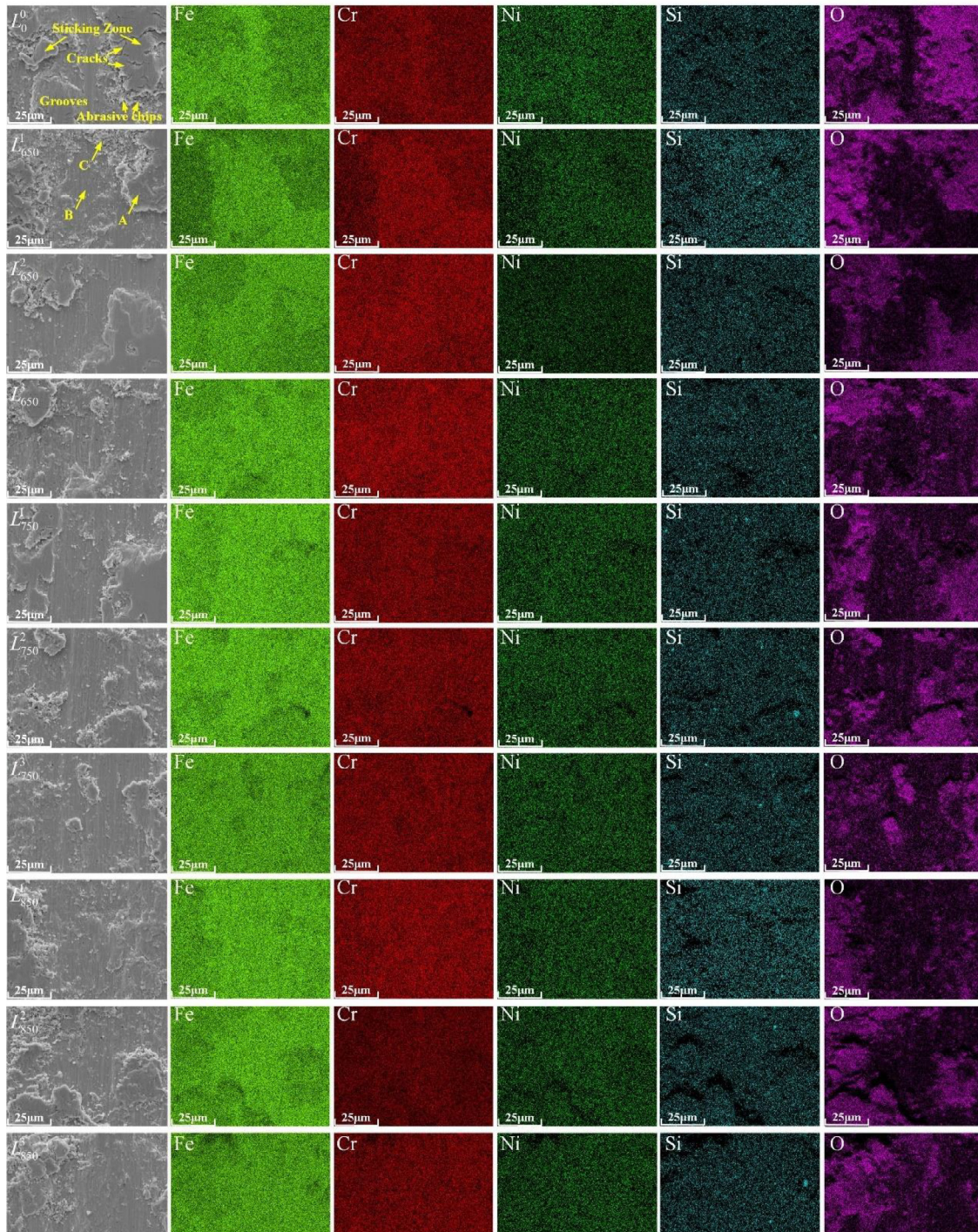


Fig. 12. Mapping scanning results of wear morphology with different remelting power and remelting times.

surface. In addition, a portion of clad layer adheres to grinding ball and then is sheared away, which result in relatively smooth planes on the wear surface. The smooth planes are oxidized and oxide films are formed under the promotion of friction heat. Therefore, abrasive wear, surface fatigue wear, adhesive wear and oxidative wear occur during the wear process.

Figs. 14 and 15 show the cross-sectional wear morphology, wear width and wear depth of  $L_0^0$  clad layer and the clad layer after remelting with different remelting power and remelting times, respectively. From Figs. 14(a) and 15, it can be seen that the wear width and wear depth of the  $L_{650}^1$  clad layer are smaller than those of the  $L_0^0$  clad layer.

However, the wear width and wear depth of both the  $L_{750}^1$  and  $L_{850}^1$  clad layers are greater than those of the  $L_0^0$  clad layer. Combined with the test results of the average microhardness of each clad layer, the average microhardness of clad layer  $L_{650}^1$  is higher than the average microhardness of clad layer  $L_0^0$ . The average microhardness of the  $L_{750}^1$  and  $L_{850}^1$  clad layers is lower than the average microhardness of the  $L_0^0$  clad layer. When the wear parameters are kept constant, the decrease in the average microhardness leads to an increase in the volume of the grinding ball embedded in the clad layer. As a result, the wear width and wear depth show a tendency to increase. In addition, it can be seen from Figs. 14(a) and 15 that when the remelting time is kept constant, the wear width

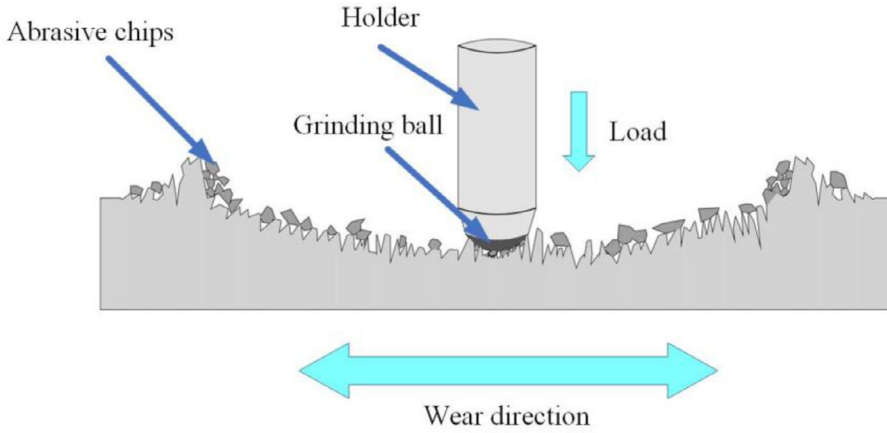


Fig. 13. Schematic diagram of the wear mechanism.

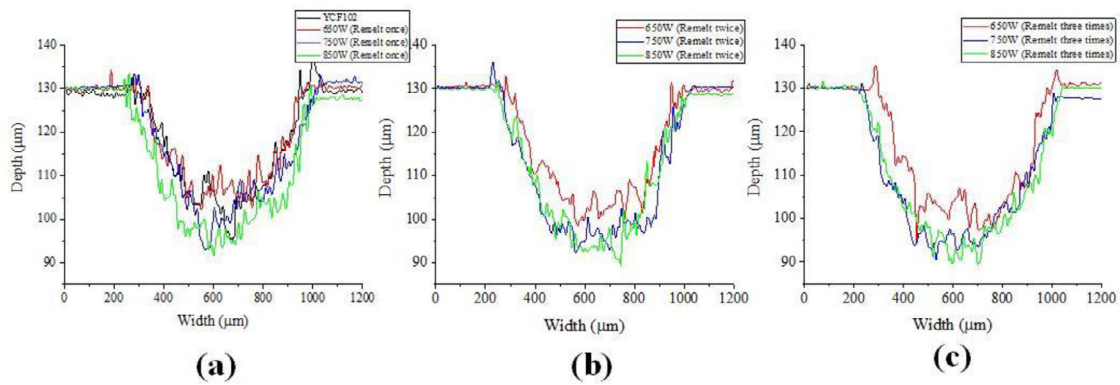


Fig. 14. Cross-sectional wear patterns of the clad layer without remelting and after remelting with different remelting times and remelting power.

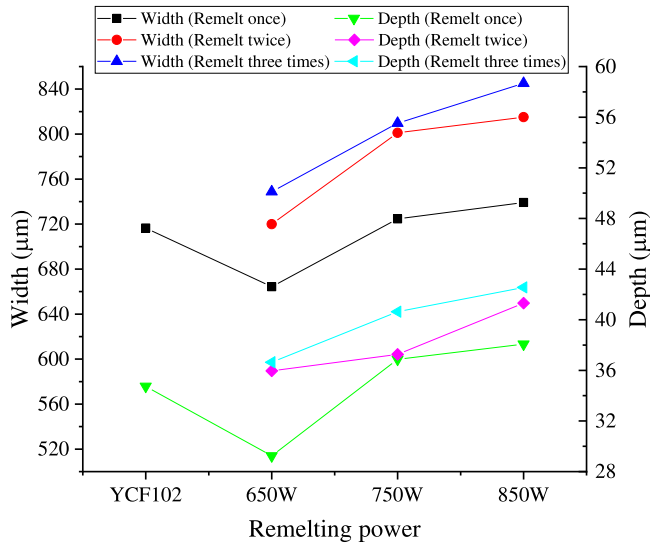


Fig. 15. Wear width and wear depth of the clad layer without remelting and after remelting with different remelting times and remelting power.

and wear depth increase with the increase of remelting power. The trend of their changes is opposite to that of the average microhardness. This result shows that the decrease in the average microhardness leads to an increase in the wear width and wear depth. From Figs. 14(b), (c) and 13, it can be seen that when the remelting power is kept constant, the

wear width and wear depth also show an increasing trend with the increase of remelting time. This phenomenon is caused by the decrease of the average microhardness with the increase of remelting time, which leads to the increase of the wear width and wear depth. At the same time, it can be seen from Figs. 14 and 15 that an increase in the remelting time or remelting power leads to an increase in the wear width and wear depth. However, changing the remelting time does not change the variation pattern of wear width and wear depth with remelting power. Likewise, changing the remelting power does not change the variation pattern of wear width and wear depth with the remelting time.

Fig. 16 shows the wear rates of the  $L_0^0$  clad layer and the clad layers after remelting with different remelting power and remelting times. From Fig. 16(a), it can be seen that when the remelting time is 1, the wear rates of the clad layers are arranged in the following order:  $L_{650}^1 < L_0^0 < L_{750}^1 < L_{850}^1$ . This result indicates that the decrease in the average microhardness leads to an increase in the wear width and wear depth, which results in an increase in the wear rate. In addition, it can be seen from Fig. 16(a)–(c) that when the remelting time is kept constant, an increase in remelting power leads to an increase in wear rate. When the remelting power is kept constant, the wear rate shows an increasing trend with the increase in the remelting time. This trend is opposite to the trend of the average microhardness and is the same as the trend of the wear width and wear depth with remelting power and remelting time. This result indicates that the average microhardness decreases with increasing remelting power or remelting time, which leads to a deterioration of wear resistance. However, changing the remelting time does not have a significant effect on the variation pattern of the wear rate with remelting power. Similarly, changing the remelting power does not have a significant effect on the variation pattern of the wear rate with the remelting time.

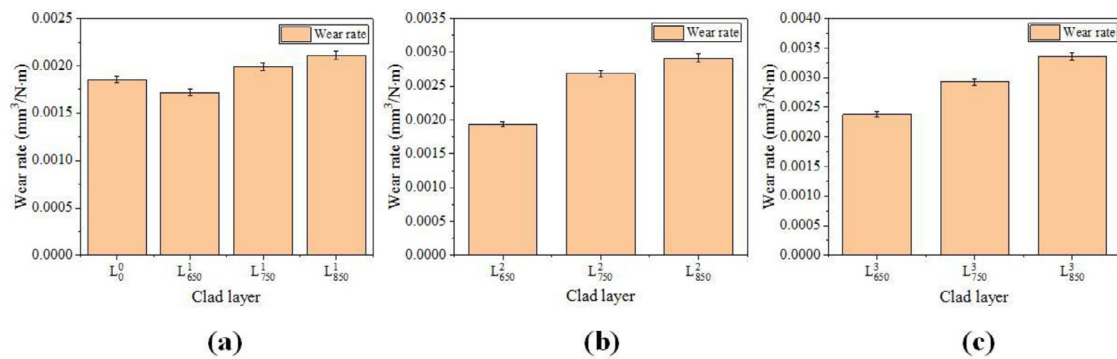


Fig. 16. Wear rate of the clad layer without remelting and after remelting with different remelting times and remelting power.

#### 4. Conclusions

Laser remelting tests with different remelting power and remelting times were conducted on YCF102 clad layer respectively, and the following conclusions were obtained:

- (1) An increase in the remelting time or remelting power leads to an increase in clad width, melting pool depth and dilution rate as well as a decrease in clad height. The clad height of the  $L_{650}^1$  clad layer is higher than that of the  $L_0^0$  clad layer, while the clad height of the clad layer after remelting with other conditions is lower than that of the  $L_0^0$  clad layer. The clad width, melting pool depth and dilution rate of the clad layer after remelting with different remelting time and remelting power conditions are greater than those of the  $L_0^0$  clad layer.
- (2) The increase of remelting time or remelting power leads to the decrease of average microhardness, increase of wear rate and deterioration of wear resistance, but it does not change the trend of average microhardness, wear rate and wear resistance with remelting power or remelting time.
- (3) The increase in the remelting time or remelting power does not change the wear forms of the clad layer, but leads to an increase in the volume of the grinding ball embedded in the clad layer and a more intense wear of the clad layer.
- (4) Under  $L_{650}^1$  condition, the clad layer has not only high microhardness, but also good wear resistance as well as low wear rate.

#### Declaration of Competing Interest

On behalf of my co-authors, I would like to declare that the work described is original research that has not previously been published. And we declare that we do not have any commercial or association interests that conflict with the submitted works.

#### CRediT authorship contribution statement

**Wenchao Xi:** Conceptualization, Investigation, Writing – original draft, Writing – review & editing. **Boxue Song:** Validation, Writing – review & editing. **Zhengyu Sun:** Validation, Writing – review & editing. **Zhelun Ma:** Validation. **Tianbiao Yu:** Resources, Supervision, Project administration, Funding acquisition. **Jun Wang:** Resources, Supervision.

#### Data availability

No data was used for the research described in the article.

#### Acknowledgments

This work is supported by 2016 Green Manufacturing System Integration Project of Ministry of Industry and Information Technology of

China [grant number 201675514]; Liaoning Provincial Key Laboratory of Large Equipment Intelligent Design and Manufacturing Technology [grant number 18006001] and Key Laboratory of Shenyang [grant number 15153100].

#### References

- [1] Yu Z, Zheng Y, Chen J, Wu C, Xu J, Lu H, et al. Effect of laser remelting processing on microstructure and mechanical properties of 17-4 PH stainless steel during laser direct metal deposition. *J Mater Process Technol* 2020;284. doi:10.1016/j.jmatprotec.2020.116738.
- [2] Mateos J, Cuetos JM, Fernández E, Vijande R. Tribological behaviour of plasma-sprayed WC coatings with and without laser remelting. *Wear* 2000;239:274–81. doi:10.1016/S0043-1648(00)00325-2.
- [3] Vastola G, Zhang G, Pei QX, Zhang YW. Modeling and control of remelting in high-energy beam additive manufacturing. *Addit Manuf* 2015;7:57–63. doi:10.1016/j.addma.2014.12.004.
- [4] Grum J, Šturm R. A new experimental technique for measuring strain and residual stresses during a laser remelting process. *J Mater Process Technol* 2004;147:351–8. doi:10.1016/j.jmatprotec.2004.01.007.
- [5] Wang Z, Tan M, Wang J, Zeng J, Zhao F, Xiao X, et al. Core-shell structural iron based metal matrix composite powder for laser cladding. *J Alloy Compd* 2021;878. doi:10.1016/j.jallcom.2021.160127.
- [6] Chen H, Lu Y, Luo D, Lai J, Liu D. Epitaxial laser deposition of single crystal Ni-based superalloys: repair of complex geometry. *J Mater Process Technol* 2020;285. doi:10.1016/j.jmatprotec.2020.116782.
- [7] Cui C, Wu M, Miao X, Gong Y, Zhao Z. The effect of laser energy density on the geometric characteristics, microstructure and corrosion resistance of Co-based coatings by laser cladding. *J Mater Res Technol* 2021;15:2405–18. doi:10.1016/j.jmrt.2021.09.073.
- [8] Yang Y, Li X, Khonsari MM, Zhu Y, Yang H. On enhancing surface wear resistance via rotating grains during selective laser melting. *Addit Manuf* 2020;36. doi:10.1016/j.addma.2020.101583.
- [9] Richter B, Chen S, Morrow JD, Sridharan K, Eriten M, Pfefferkorn FE. Pulsed laser remelting of A384 aluminum, part II: modeling of surface homogenization and topographical effects. *J Manuf Process* 2018;32:230–40. doi:10.1016/j.jmapro.2018.02.009.
- [10] Gok MG, Goller G. Microstructural evaluation of laser remelted gadolinium zirconate thermal barrier coatings. *Surf Coat Technol* 2015;276:202–9. doi:10.1016/j.surfcoat.2015.06.074.
- [11] Qunshuang M, Yajiang L, Juan W, Kun L. Homogenization of carbides in Ni60/WC composite coatings made by fiber laser remelting. *Mater Manuf Process* 2015;30:1417–24. doi:10.1080/10426914.2015.1026353.
- [12] Matějček J, Holub P. Laser remelting of plasma-sprayed tungsten coatings. *J Therm Spray Technol* 2014;23:750–4. doi:10.1007/s11666-014-0067-4.
- [13] Das B, Nath AK, Bandyopadhyay PP. Online monitoring of laser remelting of plasma sprayed coatings to study the effect of cooling rate on residual stress and mechanical properties. *Ceram Int* 2018;44:7524–34. doi:10.1016/j.ceramint.2018.01.152.
- [14] Gao W, Zhao S, Wang Y, Liu F, Zhou C, Lin X. Effect of re-melting on the cladding coating of Fe-based composite powder. *Mater Des* 2014;64:490–6. doi:10.1016/j.matdes.2014.08.004.
- [15] Amaya-Vazquez MR, Sánchez-Amaya JM, Boukha Z, Botana FJ. Microstructure, microhardness and corrosion resistance of remelted TiG2 and Ti6Al4V by a high power diode laser. *Corros Sci* 2012;56:36–48. doi:10.1016/j.corsci.2011.11.006.
- [16] Wang QY, Bai SL, Zhang YF, De Liu Z. Improvement of Ni-Cr-Mo coating performance by laser cladding combined re-melting. *Appl Surf Sci* 2014;308:285–92. doi:10.1016/j.apsusc.2014.04.156.
- [17] Wang HZ, Cheng YH, Yang JY, Wang QQ. Influence of laser remelting on organization, mechanical properties and corrosion resistance of Fe-based amorphous composite coating. *Surf Coat Technol* 2021;414. doi:10.1016/j.surfcoat.2021.127081.
- [18] Tian YS, Chen CZ, Li ST, Huo QH. Research progress on laser surface modification of titanium alloys. *Appl Surf Sci* 2005;242:177–84. doi:10.1016/j.apsusc.2004.08.011.

- [19] Pariona MM, Teleginski V, Santos K, Dos Dos, Santos ELR, De Oliveira Carmargo De Lima AA, Riva R. AFM study of the effects of laser surface remelting on the morphology of Al-Fe aerospace alloys. *Mater Charact* 2012;74:64–76. doi:[10.1016/j.matchar.2012.08.011](https://doi.org/10.1016/j.matchar.2012.08.011).
- [20] Iwaszko J. Surface remelting treatment of plasma-sprayed Al<sub>2</sub>O<sub>3</sub> + 13 wt.% TiO<sub>2</sub> coatings. *Surf Coat Technol* 2006;201:3443–51. doi:[10.1016/j.surfcoat.2006.07.234](https://doi.org/10.1016/j.surfcoat.2006.07.234).
- [21] Cai Z, Cui X, Liu Z, Li Y, Dong M, Jin G. Microstructure and wear resistance of laser clad Ni-Cr-Co-Ti-V high-entropy alloy coating after laser remelting processing. *Opt Laser Technol* 2018;99:276–81. doi:[10.1016/j.optlastec.2017.09.012](https://doi.org/10.1016/j.optlastec.2017.09.012).
- [22] Habib KA, Cano DL, Heredia JA, Mira JS. Effect of post-coating technique on microstructure, microhardness and the mixed lubrication regime parameters of thermally-sprayed NiCrBSi coatings. *Surf Coat Technol* 2019;358:824–32. doi:[10.1016/j.surfcoat.2018.12.004](https://doi.org/10.1016/j.surfcoat.2018.12.004).
- [23] Cai Y, Cui Y, Zhu L, Tian R, Geng K, Li H, et al. Enhancing the (FeMnCr-NiCo + TiC) cladding layer by *in-situ* laser remelting. *Surf Eng* 2021;37:1496–502. doi:[10.1080/02670844.2020.1868651](https://doi.org/10.1080/02670844.2020.1868651).
- [24] Mukherjee S, Dhara S, Saha P. Laser surface remelting of Ti and its alloys for improving surface biocompatibility of orthopaedic implants. *Mater Technol* 2018;33:106–18. doi:[10.1080/10667857.2017.1390931](https://doi.org/10.1080/10667857.2017.1390931).
- [25] Gao YL, Wang CS, Yao M, Liu HB. The resistance to wear and corrosion of laser-cladding Al<sub>2</sub>O<sub>3</sub> ceramic coating on Mg alloy. *Appl Surf Sci* 2007;253:5306–11. doi:[10.1016/j.apsusc.2006.12.001](https://doi.org/10.1016/j.apsusc.2006.12.001).
- [26] Ciubotariu CR, Frunzaverde D, Mărginean G, Serban VA, Birdeanu AV. Optimization of the laser remelting process for HVOF-sprayed Stellite 6 wear resistant coatings. *Opt Laser Technol* 2016;77:98–103. doi:[10.1016/j.optlastec.2015.09.005](https://doi.org/10.1016/j.optlastec.2015.09.005).
- [27] Xi W, Song B, Wang Z, Yu T, Wang J, Dai Y. Effect of laser re-melting on geometry and mechanical properties of YCF102 cladding layer. *Surf Coat Technol* 2021;408. doi:[10.1016/j.surfcoat.2020.126789](https://doi.org/10.1016/j.surfcoat.2020.126789).
- [28] Pereira D, Gandra J, Pamies-Teixeira J, Miranda RM, Vilaça P. Wear behaviour of steel coatings produced by friction surfacing. *J Mater Process Technol* 2014;214:2858–68. doi:[10.1016/j.jmatprotec.2014.06.003](https://doi.org/10.1016/j.jmatprotec.2014.06.003).